Int. J. Heat Mass Transfer. Vol. 36, No. 6, pp. 1609–1617, 1993
Printed in Great Britain

0017-9310/93 $6.00 + 0.00
Pergamon Press Ltd

Numerical and experimental analysis of laminar fluid flow and forced convection heat transfer in a grooved duct

BIJAN FARHANIEH,† ČILA HERMAN‡ and BENGT SUNDÉN†

† Department of Thermo- and Fluid Dynamics, Chalmers University of Technology, 412 96 Göteborg, Sweden

‡ Lehrstuhl A für Thermodynamik, TU München, Arcisstraße 21, 8000 München 2, Germany

(*Received* 9 *June* 1992)

Abstract—A numerical and experimental investigation of laminar fluid flow and heat transfer characteristics in a duct with a grooved wall is presented. The plane wall of the duct is kept cold whereas the grooved wall is heated and kept at a uniform temperature. In the experiments, holographic interferometry was applied. The visualized temperature fields were used to reconstruct temperature profiles and from these heat transfer coefficients were evaluated. The governing equations are solved numerically by a finite-volume method for elliptic flows. The results are obtained for Reynolds number ranging from 100 to 1760. The numerically calculated local Nusselt numbers are in good agreement with the obtained experimental values. The streamline plots explain the influence of the fluid flow on the Nusselt number and the pressure drop. The local Nusselt number increases by increasing the Reynolds number. However, the pressure drop penalty was high.

1. INTRODUCTION

HEAT TRANSFER in parallel plates and rectangular ducts has been reviewed in the literature, e.g. Shah and London [1], and Shah and Bhatti [2]. In engineering applications, enhancement of the thermal performance of heat transfer devices is attempted. Compact heat exchangers and cooling of electronics exemplify such applications. One way of improving the performance of a parallel plate duct is to introduce transversal grooves, which periodically interrupt the heat transfer surface. The flow separates and a periodical redevelopment of the thermal boundary layer occurs. The heat transfer coefficient may then be higher than that for the parallel plate duct. Reviews of the relevant literature have been presented by Herman and Mayinger [3, 4].

The purpose of the present collaborative work is to experimentally and numerically investigate the thermal characteristics of a specific grooved parallel plate duct.

2. PROBLEM UNDER CONSIDERATION

The duct considered is presented schematically in Fig. 1. The geometry of the duct is specified by the groove width w, groove height h and the hydraulic diameter ($D_h = 6h$). The heat transfer and fluid flow characteristics for laminar, incompressible, forced convection along the duct are to be determined. The walls of the duct are kept at uniform but different temperatures. The plane wall is the cold one and the grooved wall is the heated one. The aspect ratios of the duct are groove width/duct height = 4:1 and duct height/groove height = 2:1. The main flow is in the x-direction.

3. EXPERIMENTAL ARRANGEMENT AND INSTRUMENTATION

3.1. *Experimental arrangement*

The experimental arrangement used in the visualization of temperature fields is presented schematically in Fig. 2. The experimental channel is in the vertical position and it consists of the entry section, the test section and the exit section. The entry section is a 0.9 m long, $2h = 0.01$ m high and $d = 0.22$ m wide rectangular duct. The selected length of the entry section provides the fully developed velocity profiles at the entrance of the test section. The width-to-height ratio (22:1) is needed to obtain the essentially two-dimensional temperature distribution, significant for an accurate reconstruction of temperature fields from interferograms. The test section is 0.22 m long and both its walls, made of aluminium, are provided with water channels. Circulating water from two constant temperature water baths, in three parallel loops for each channel wall, maintains uniform wall temperatures. The plane cold wall is kept at ambient temperature and the grooved wall is heated to a temperature which is ΔT above the value for the cold wall. The length of the grooves w is 0.02 m and their depth h is 0.005 m. Glass windows allow for the transillumination of the investigated region. The exit section is 0.3 m long, so that it removes possible down-

NOMENCLATURE

d	width of the duct
D_h	hydraulic diameter
h	height of the groove
k	thermal conductivity of the fluid
L	length of the transilluminated region
n	refractive index of air
N	molar refractivity
Nu_x	local Nusselt number
p	pressure
P	dimensionless pressure
Pr	Prandtl number
q_w	heat flux
R	universal gas constant
Re	Reynolds number
S	interference order
T	temperature
T_b	bulk temperature
T_c	temperature of the cold wall
T_h	temperature of the hot wall
T_{in}	inlet temperature
T_w	wall temperature
u_m	mean velocity
U	dimensionless axial velocity
V	dimensionless velocity in the y-direction
w	width of the groove
x	coordinate
X	dimensionless streamwise coordinate
y	coordinate
Y	dimensionless coordinate
z	coordinate.

Greek symbols

α	heat transfer coefficient
ΔP	pressure drop in grooved duct
ΔP_0	pressure drop in parallel plate duct
δY_j	height of the control volume
η	distance normal to the wall
Θ	dimensionless temperature
Θ_b	dimensionless bulk temperature
λ	wavelength of laser light
μ	dynamic viscosity
ρ	density.

stream effects from the test section, and it carries the blower creating the air flow. The blower is operating in a suction mode, and the flow velocity is varied by varying the d.c. supply voltage of the blower.

3.2. *Instrumentation*

Flow velocity profile measurements were taken by a Schiltknecht hot wire anemometer thermo air type 442 calibrated by a rotameter. From the measured

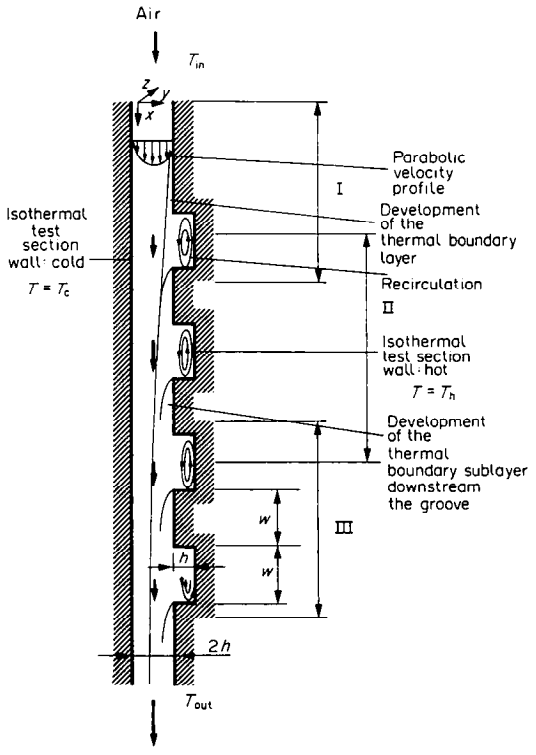

FIG. 1. Schematic diagram of the investigated geometry and the physical situation.

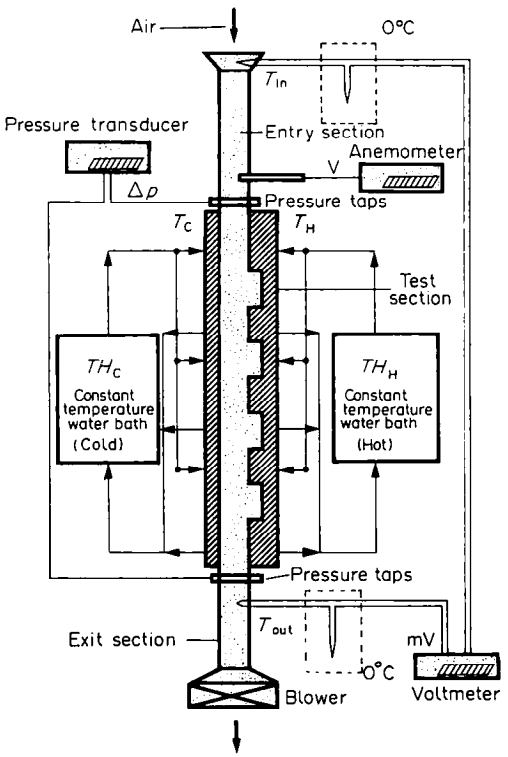

FIG. 2. Schematic diagram of the experimental arrangement.

velocity profiles, the cross channel average flow velocity u_m was evaluated with an estimated uncertainty of 7%. The temperatures of the hot wall and of the cold wall were monitored by 25 nickelchrome–constantan thermocouples, providing reference values for the interferometric measurements.

3.3. *Measuring technique*

The method of holographic interferometry was used in the visualization of temperature fields in the experiments described in this paper. Being a non-invasive method it is well suited for measurements in complex geometries as it does not disturb the investigated phenomenon. By means of holographic interferometry, qualitative information on the temperature fields and—by evaluating the images–quantitative heat transfer data can also be obtained.

The optical set-up used in the measurements is presented schematically in Fig. 3. In the experiments, a 5 W Argon-ion-laser with $\lambda = 514.5$ nm wavelength and 0.5 m coherence length was used as the light source. The interferograms were obtained using the real time method: the reference state with the test section at ambient temperature is recorded first on the holographic plate which is then processed and accurately repositioned into its original position. Then the investigated process started; the test section walls are brought to the desired temperature and air flow is created by the blower. The interferograms were recorded on photographic film, and the processed negatives were then analysed and measured by a photometer. Since the test section is longer (0.22 m) than the diameter of the expanded laser beam (0.078 m), the temperature fields were recorded at three different heights of the test section (indicated by I, II and III in Fig. 1) in different experimental runs.

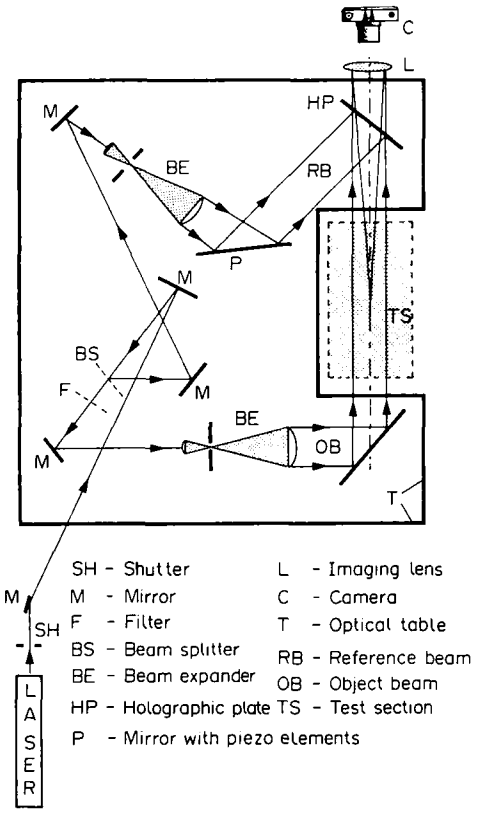

FIG. 3. Schematic diagram of the optical arrangement for holographic interferometry.

In the evaluation of the interferograms, the phase difference, visualized by light and dark fringes and expressed as a multiple of the wavelength of light λ, can be evaluated as the difference between the optical path of the measuring beam (index M) and the reference beam (index R) as

$$S(x,y)\cdot\lambda = L\cdot\{n(x,y)_M - n(x,y)_R\}, \qquad (1)$$

where L is the length of transilluminated region (length of the test section) and n the refractive index.

Intensity minima are obtained for

$$|S| = \tfrac{1}{2};\tfrac{3}{2};\tfrac{5}{2};\ldots \text{(dark fringes)} \qquad (2)$$

and intensity maxima for

$$|S| = 0;1;2;3;\ldots \text{(light fringes)}. \qquad (3)$$

As the refractive index field for the reference beam is known, the two-dimensional refractive index field can be evaluated from the interferograms as follows if $n_R(x,y) = n_x = \text{constant}$:

$$S(x,y)\cdot\lambda = L\cdot\{n(x,y)_M - n_x\}. \qquad (4)$$

By combining the ideal gas equation of state and the Gladstone–Dale equation, the temperature corresponding to a certain fringe shift can be evaluated as

$$T(x,y) = \left[\frac{S(x,y)2\lambda R}{3N(\lambda)pL} + \frac{1}{T_x}\right]^{-1}. \qquad (5)$$

In this equation, R is the universal gas constant, p the pressure and N the molar refractivity. More details about the reconstruction procedure are given in the literature [5].

In the evaluation of temperature profiles from the interferometric image, uncertainties are introduced mainly through the influence of the viewing window; the influence of uncertainties is smaller in the determination of the location of the fringe extreme and the misalignment of the test section and the expanded laser beam. The effects of the uncertainties in the determination of wall positions are negligible. Calculations have shown that the parabolic approximation provides sufficient accuracy in the reconstruction of the temperature profiles for the temperature gradients present in these measurements. The temperature values obtained in the interferometric measurements were compared with control thermocouple readings, and the maximum deviation was found to be in the range of 7%. However, in most of the measurements the deviation was found to be in

the range of 2–3%. The local Nusselt numbers are evaluated from the temperature gradients on the heated walls with a maximum uncertainty of 8.5%, depending on the uncertainty of the temperature measurements.

4. GOVERNING EQUATIONS

The governing equations are the continuity, momentum and energy equations. The flow is studied under the following assumptions: steady state, constant fluid properties, negligible viscous dissipation and no natural convection. The following dimensionless variables are introduced:

$$X_i = \frac{x_i}{D_h} \quad U_i = \frac{u_i}{u_m} \quad P = \frac{p}{\rho u_m^2} \quad \theta = \frac{T - T_{in}}{T_w - T_{in}}.$$

The governing equations take the following non-dimensional form:

$$\frac{\partial U}{\partial X} + \frac{\partial V}{\partial Y} = 0 \tag{6}$$

$$U\frac{\partial U}{\partial X} + V\frac{\partial U}{\partial Y} = -\frac{\partial P}{\partial X} + \frac{1}{Re}\nabla^2 U \tag{7}$$

$$U\frac{\partial V}{\partial X} + V\frac{\partial V}{\partial Y} = -\frac{\partial P}{\partial Y} + \frac{1}{Re}\nabla^2 V \tag{8}$$

$$U\frac{\partial \Theta}{\partial X} + V\frac{\partial \Theta}{\partial Y} = \frac{1}{Pr\,Re}\nabla^2 \Theta. \tag{9}$$

5. NUMERICAL SOLUTION PROCEDURE

A general-purpose finite-volume method using boundary fitted coordinates was employed although Cartesian coordinates suffice in this case.

The momentum equations are solved for the velocity components U and V in the fixed Cartesian directions on a non-staggered grid. All the variables are thus stored at the centre of the control volume. The velocity components at the control volume faces are computed by the Rhie–Chow interpolation method and the pressure–velocity coupling is handled by the SIMPLEC method. The convective terms are treated by the hybrid upwind/central difference scheme whereas the diffusive terms are treated by a central difference scheme. TDMA-based algorithms are applied for solving the algebraic equations. Further details are provided by Davidson and Farhanieh [6] and the earlier papers by Farhanieh and Sundén [7, 8].

5.1. *Pressure drop*

The cross-sectional average pressure at the inlet and outlet is obtained by

$$\bar{P} = \frac{\sum_1^N P_j \delta Y_j}{2h}, \tag{10}$$

where δY_j is the height of the control volume in the y-direction.

For practical applications, it is desirable to compare the pressure drop with corresponding values for straight parallel plate duct flow with the hydraulic diameter $D_h = 6h$. In standard textbooks on fluid mechanics, e.g. White [9], the pressure drop Δp in a straight parallel plate duct is expressed as

$$\Delta p_{pd} = \frac{96}{Re}\frac{L}{D_h}\frac{\rho u_m^2}{2}, \tag{11}$$

where

$$Re = \frac{\rho u_m D_h}{\mu}. \tag{12}$$

Subscript pd refers to the straight parallel plate duct.

5.2. *Nusselt number*

The heat transfer results are expressed in terms of the dimensionless Nusselt number. The local heat flux, q_w, is defined as

$$q_w = -k\left(\frac{\partial T}{\partial \eta}\right)_{w,x} = \alpha(T_w - T_b), \tag{13}$$

where $(\partial T/\partial \eta)_{w,x}$ is the temperature gradient normal to the wall at any cross-sectional position x along the duct, α is the heat transfer coefficient, and k the thermal conductivity of the fluid. The Nusselt number is defined as

$$Nu = \frac{\alpha D_h}{k}. \tag{14}$$

By introducing equation (13) in equation (14) and using the non-dimensional temperature Θ, we obtain

$$Nu_x = \frac{D_h\left(\frac{\partial \Theta}{\partial Y}\right)_{w,x}}{(1 - \Theta_b)}, \tag{15}$$

where Θ_b is the local dimensionless bulk temperature and is given by

$$\Theta_b = \frac{\int_0^Y |U|\Theta\, dY}{\int_0^Y |U|\, dY}. \tag{16}$$

In engineering practice, the average bulk temperature is calculated by a simple approximate average value

$$\Theta_{b_{av}} = \frac{\Theta_{inlet} + \Theta_{outlet}}{2}. \tag{17}$$

The boundary conditions at the walls are $U = V = 0$, $\Theta = 1$ (at the heated wall) and $\Theta = 0$ (at the cold wall and the inlet). At the inlet, the velocity field is assumed to be fully developed and the temperature field is uniform, i.e. $\Theta = 0$. The condition of zero gradients is imposed at the outlet.

Table 1. Grid size effect on pressure drop

Grid size	$(\Delta P/\Delta P_{pd})$
89 × 20	1.125
112 × 26	1.515
112 × 32	1.527
112 × 46	1.531
136 × 32	1.508
156 × 32	1.501

5.3. *Computational details*

The Prandtl number was set equal to 0.72 and the Reynolds number was varied from 100 to 1760. The solution procedure is iterative for all variables and the computations were terminated when the sum of absolute residuals normalized by the inflow fluxes were below 10^{-4} for all the variables. To achieve convergence in the solution, an under-relaxation factor of 0.5 was chosen for all the variables.

5.4. *Grid size effects and numerical accuracy*

The grid points are distributed in a non-uniform manner with a higher concentration of grid points close to the walls. Each control volume contains one node at its centre but the boundary adjacent volumes contain two nodes.

Accuracy tests were performed on the numerical procedure, particularly to study the effect of the grid fineness on the solution. Comparison of the pressure drop and the local Nusselt numbers under various grid sizes were made and are listed and presented in Table 1 and Fig. 4, respectively. The results show that by increasing the fineness of the grid no significant changes appear in the local Nusselt number values. The changes in the pressure drop values were also small.

To further assess the accuracy of the computational technique, calculations have previously been carried out for various ducts for which analytical and experimental data are available. So, for instance, the comparison of the Nusselt number and friction factor in fully developed laminar flow in square ducts agreed well with the analytical results (within 0.17% and 0.32%, respectively) obtained by Shah and London [1]. The reader is referred to ref. [7] for details.

All calculations were carried out on a DEC 3100 work-station.

6. RESULTS AND DISCUSSION

6.1. *Flow and temperature fields*

The effects of Reynolds number on the flow field in the duct for five different Reynolds numbers are presented in Fig. 5. The streamline maps in Fig. 5 give a qualitative understanding of the fluid flow pattern in the duct under consideration. At low *Re*, the flow occupies the front part of the grooves and formation of separation bubbles can be observed at the upstream part of the grooves. The streamlines are deflected into the grooves. As the Reynolds number increases, the separation bubbles grow larger and the streamlines of the main stream become straight. The flow patterns tend to be unchanged from the second groove onwards, indicating the establishment of fully developed periodic flow.

Figure 6 shows typical interferogram sets recorded at different flow velocities using the infinite fringe field arrangement. The average temperature difference between the hot wall and cold wall is $\Delta T \approx 30$ K. Fringes correspond to isotherms with ΔT/fringe pair ≈ 3 K. Air flows from left to right in this figure. As the flow velocity is increased the temperature gradient becomes steeper at the straight narrow parts of

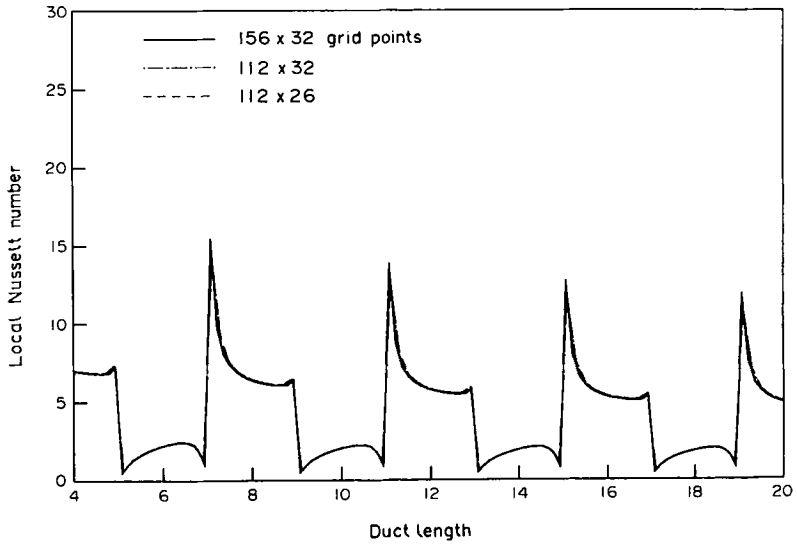

FIG. 4. Effect of grid size on local Nusselt number.

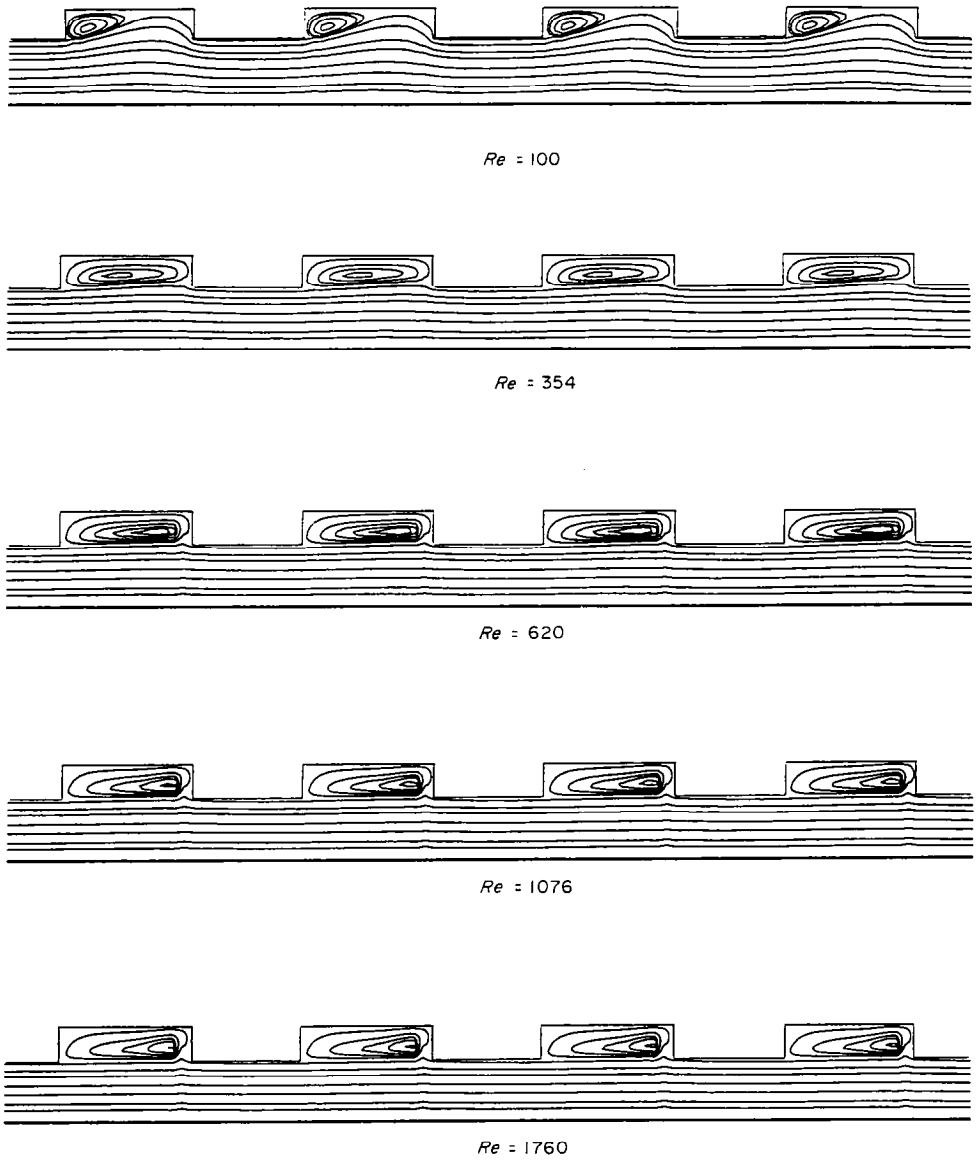

FIG. 5. Streamline maps for five different Reynolds numbers.

the duct, while in the grooves only minor effects occur as the flow velocity is increased. The bottom interferogram set corresponds to natural convection since no flow is forced through the channel. It should be remembered that the test channel is placed vertically and not horizontally as shown in Fig. 6.

A comparison of the computed isotherms with experimental ones for two different Reynolds numbers is presented in Fig. 7. The agreement is satisfactory.

6.2. *Pressure drop*

Results for the pressure drop ratio versus Reynolds numbers are presented in Fig. 8. The ratio is determined numerically by dividing ΔP for the grooved duct by the corresponding value for a parallel plate duct with a height equal to $3h$. This figure should be studied in conjunction with the streamlines map. The pressure drop ratio increases as the Reynolds number increases and reaches a maximum at $Re \approx 600$; thereafter the pressure drop ratio decreases with increasing Reynolds number. The decrease in the pessure drop ratio halts at $Re \approx 1000$ and a very moderate increase in pressure drop ratio can be observed after that. The pressure drop of the grooved duct is always greater than that of the smooth duct.

6.3. *Local Nusselt number*

Distributions of the experimental and numerical local Nusselt number (Nu_x) along the heated wall were obtained for four different Reynolds numbers and are plotted in Fig. 9. A comparison of the local Nusselt numbers for four different Reynolds numbers is pre-

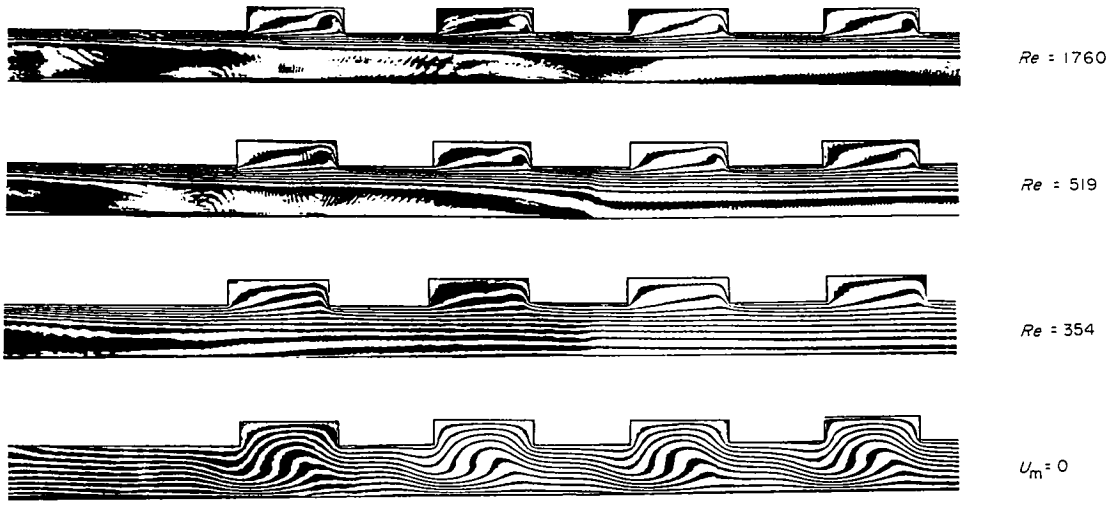

FIG. 6. Interferogram sets for four different Reynolds numbers.

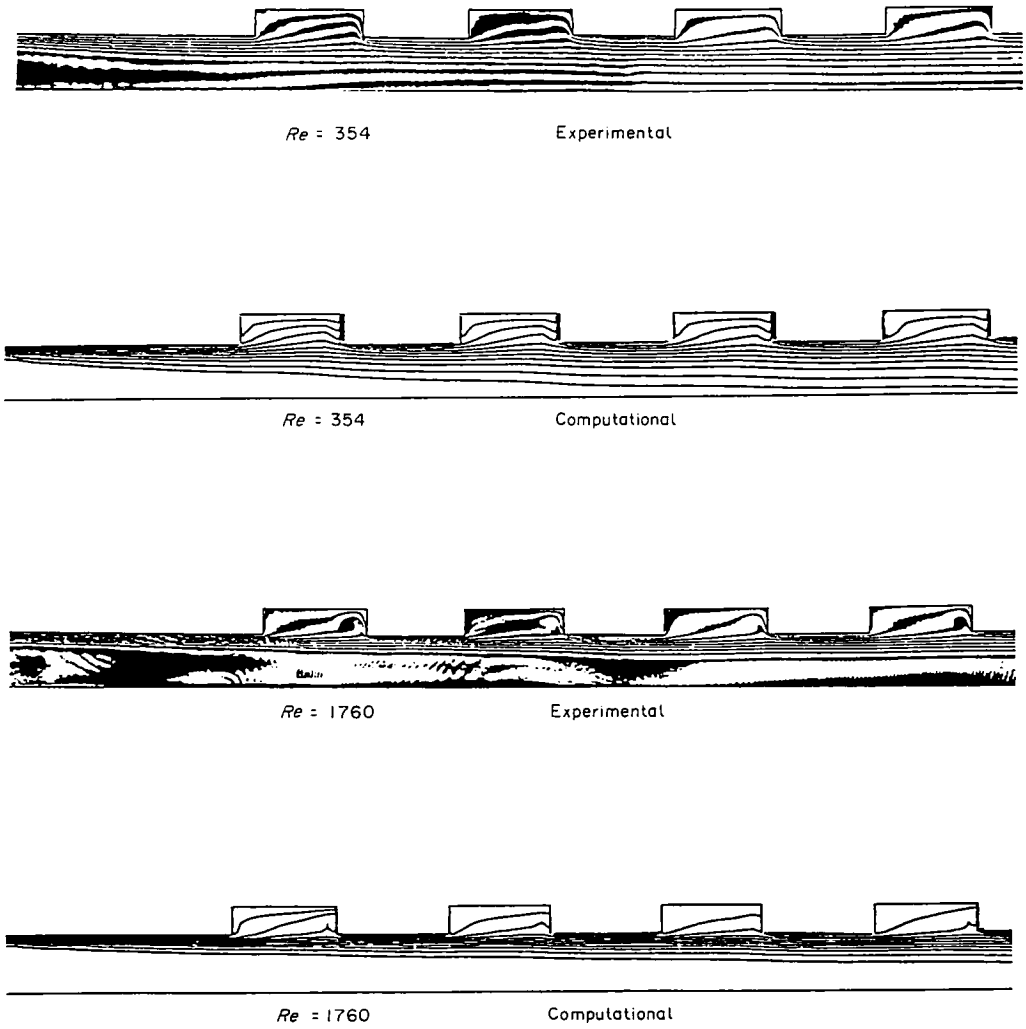

FIG. 7. Comparison of the numerical calculations with experimental results.

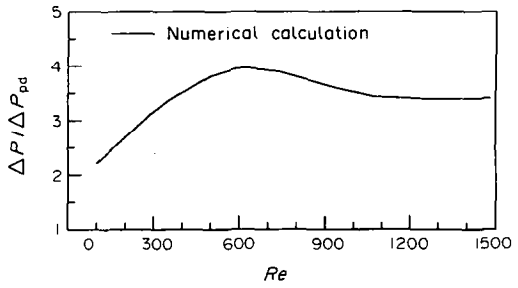

FIG. 8. Pressure drop vs Reynolds number.

sented in Fig. 10. These figures should be studied in conjunction with Fig. 5. The agreement between computations and experiments is quite good. The local Nusselt number shows the same characteristic behaviour for all four values of the Reynolds number. Immediately at the beginning of the first groove the local Nusselt number falls sharply. This is due to the low flow velocities in the recirculating zone. Within the groove it increases gradually and reaches a maximum value at the last quarter section of the groove. After this peak the value of the local Nusselt number falls sharply near the rear wall of the groove. Due to the low convective velocities inside the grooves, the values of the local Nusselt number in the grooves are lower than in the main duct. Immediately downstream of the groove, Nu_x reaches a sharp maximum. This peak is followed by a gradual decrease along the straight section towards the next groove. This behaviour corresponds to re-establishment of thermal boundary layers.

By increasing the Reynolds number, the values of Nu_x increase everywhere except inside the first three quarters of the groove. In this region the local Nusselt

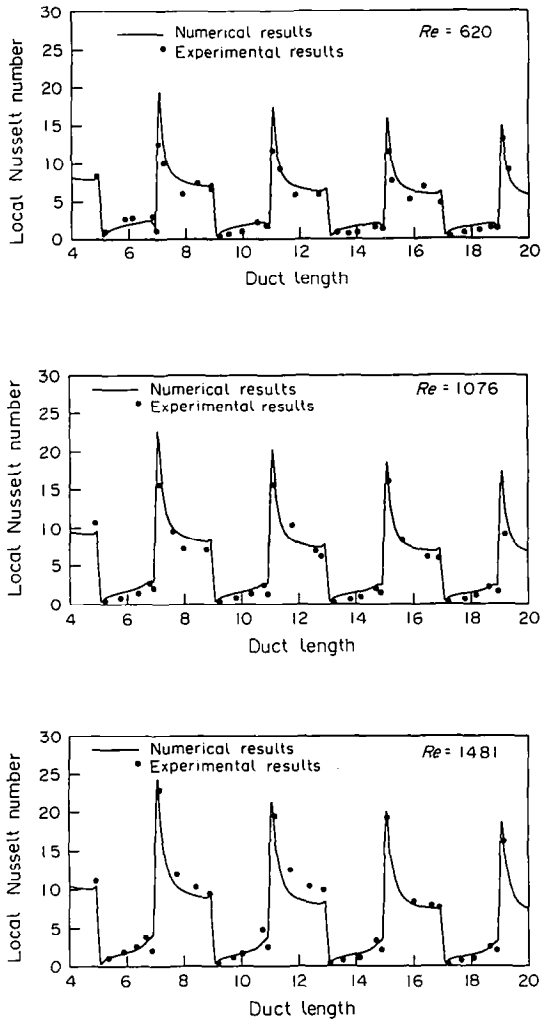

FIG. 9. Comparison of computational and experimental local Nusselt numbers.

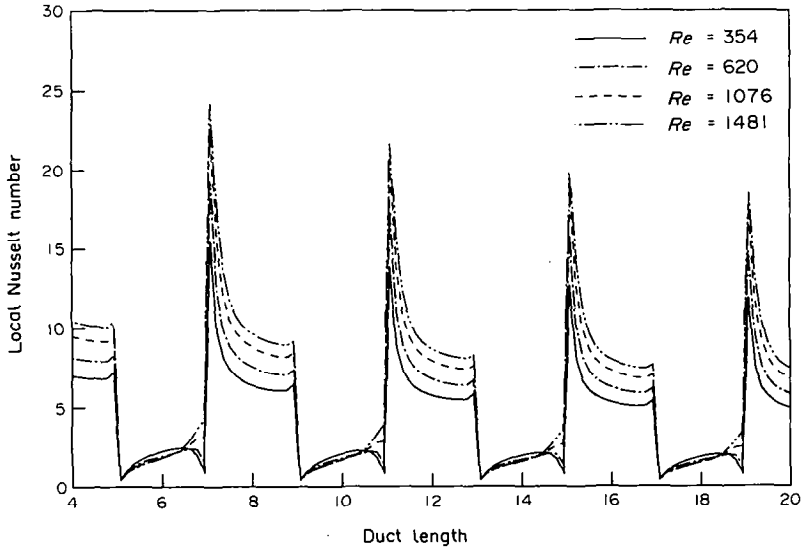

FIG. 10. Local Nusselt number along the duct with Re as parameter.

number decreases slightly as the Reynolds number increases.

7. CONCLUSIONS

The numerical and experimental results indicate enhancement in the local Nusselt number compared with a straight parallel plate duct. Heat transfer in the main duct region is related to re-establishment of thermal boundary layers and its contribution is the most significant part of the total heat transfer. Inside the grooves the heat transfer is influenced by the slow recirculating flow, and the temperature gradients at the heated wall are small. The local Nusselt number increases as the Reynolds number increases. The enhancement in Nusselt number is accompanied by a relatively high pressure drop increase.

Acknowledgements—The financial support from the National Swedish Board for Technical Development (STU) and Lehrstuhl A für Thermodynamik, TU München is gratefully acknowledged.

REFERENCES

1. R. K. Shah and A. L. London, *Laminar Flow Forced Convection in Ducts*. Academic Press, New York (1978).
2. R. K. Shah and M. S. Bhatti, Laminar convective heat transfer in ducts. In *Handbook of Single-phase Convective Heat Transfer* (Edited by S. Kakaç, R. K. Shah and W. Aung), pp. 3.1–3.137. Wiley-Interscience, New York (1987).
3. C. V. Herman and F. Mayinger, Experimental investigation of the heat transfer in laminar forced convection flow in a grooved channel. In *Heat Transfer* (Edited by G. Hetsroni), **90,** Vol. 3, pp. 387–392. Hemisphere, New York (1990).
4. C. V. Herman and F. Mayinger, Interferometric study of heat transfer in a grooved geometry. In *Experimental Heat Transfer, Fluid Mechanics, and Thermodynamics 1991* (Edited by J. F. Keffer, R. K. Shah and E. N. Ganic), pp. 522–529. Elsevier, New York (1991).
5. W. Hauf and U. Grigull, Optical methods in heat transfer. In *Advances in Heat Transfer* (Edited by J. P. Hartnett and T. F. Irvine, Jr.), Vol. 6, pp. 133–366. Academic Press, New York (1970).
6. L. Davidson and B. Farhanieh, A finite-volume code employing collocated variable arrangement and cartesian velocity components for computation of heat and mass transfer in complex three-dimensional geometries, Publication no. 91/14 ISSN 1101–9972, Dept. of Thermo- and Fluid Dynamics, Chalmers University of Technology, Göteborg, Sweden (1991).
7. B. Farhanieh and B. Sundén, Three dimensional laminar flow and heat transfer in the entrance region of trapezoidal ducts, *Int. J. Numer. Meth. Fluids* **13,** 537–556 (1991).
8. B. Farhanieh and B. Sundén, Numerical investigation of periodic laminar heat transfer and fluid flow characteristics in parallel plate ducts with streamwise-periodic cavities, *Int. J. Numer. Meth. Heat Fluid Flow* **1,** 143–157 (1991).
9. F. M. White, *Fluid Mechanics* (2nd Edn), p. 331. McGraw-Hill, Singapore (1987).